

## Article

# Evaluation and Characterization of the Use of Industrial-Solid-Waste Curing Agent instead of Cement on Improved Alluvial Silt

Quanjun Shen <sup>1</sup>, Peng Jiang <sup>2,\*</sup> , Xiaoning Zhang <sup>2,\*</sup>, Hao Sun <sup>2</sup>, Yaohui Yang <sup>1</sup>, Shuai Wang <sup>2</sup>, Li Li <sup>1</sup> and Hongfa Shang <sup>1</sup>

<sup>1</sup> Shandong Hi-Speed Group Co., Ltd., Innovation Research Institute, Jinan 250098, China

<sup>2</sup> School of Civil Engineering, Shandong University, Jinan 250061, China

\* Correspondence: jiangp2020@163.com (P.J.); sdjtuzxn@163.com (X.Z.)

**Abstract:** The silt in the Yellow River alluvial plain typically features low strength and poor water stability, and, thus, alluvial silt treatment needs an amount of cement to improve soil performance. The development of an alternative to reduce or replace the use of cement in soil stabilization has been a hot topic research for a long time. This paper develops an industrial-solid-waste (ISW) curing agent using a response surface methodology, which is a novel composite material made of steel slag, mineral slag, and two desulfurization products; its feasibility on improved silt is expected to be studied systematically. The comparative tests of ISW- and cement-improved silt were conducted to analyze performance and action mechanism. Variance and multiple regression analysis were used to study the effect of factors on responses statistically, and check the significance and correlation of the suggested models. Finally, the in-service performance of ISW-improved silt was evaluated through in-situ tests. Results show that ISW-improved silt can present good mechanical properties and durability, but is much weaker than cement-improved silt in the early curing stage. The strength enhancement amplitude of ISW-improved silt between curing ages of 7 days to 28 days is larger than that of cement-improved silt. The correlation between factors and responses is established with good agreement. Synergisms in the ISW curing agent are stimulated in the alkaline environment, and are conducive to connect the silt particles. The in-service performance of ISW-improved silt showed little difference to that of cement-improved silt; both of them meet the requirements from the perspective of in-situ application. Moreover, the unit cost of an ISW curing agent is less than 1/5 of that of cement. ISW-improved silt has advantages of cost saving, resource recycling and environmental protection.

**Keywords:** alluvial silt; ISW curing agent; macro and micro test; multiple regression analysis; field application evaluation



**Citation:** Shen, Q.; Jiang, P.; Zhang, X.; Sun, H.; Yang, Y.; Wang, S.; Li, L.; Shang, H. Evaluation and Characterization of the Use of Industrial-Solid-Waste Curing Agent instead of Cement on Improved Alluvial Silt. *Coatings* **2022**, *12*, 1417. <https://doi.org/10.3390/coatings12101417>

Academic Editors: Andrea Nobili and Qiao Dong

Received: 16 September 2022

Accepted: 20 September 2022

Published: 27 September 2022

**Publisher's Note:** MDPI stays neutral with regard to jurisdictional claims in published maps and institutional affiliations.



**Copyright:** © 2022 by the authors. Licensee MDPI, Basel, Switzerland. This article is an open access article distributed under the terms and conditions of the Creative Commons Attribution (CC BY) license (<https://creativecommons.org/licenses/by/4.0/>).

## 1. Introduction

The Yellow River alluvial plain (YRAP) is located in the northwest and southwest of Shandong Province, China [1], which covers an area of 63,200 km<sup>2</sup> (Figure 1a). This privileged geographical position and abundant natural resources prompted people to settle in this area very early [2]. A large population and active economy in this area have generated strong demands for transportation facilities, especially highway engineering [3]. However, the YRAP consists mainly of alluvial silty soils, which are typically employed as backfill for subgrade construction due to the deficiency of coarse-grained soils [4]. It has the characteristics of high roundness of particle grinding (Figure 1b), low liquid limit, low cohesion and poor water stability. In addition, the groundwater level in this area often tends to be high; a strong capillary effect in alluvial silt brings 85% of in-service subgrades to an over-wet state [5]. At the same time, the YRAP is situated in a seasonally frozen region [6], and the moisture migration in subgrade soil easily leads to water accumulation during freeze–thaw cycles [7,8]. Under the influence of two above-mentioned conditions,

the increase in moisture content (Figure 1c) and the reduction in the stiffness, strength and durability of subgrades directly affects the subgrade stability and threatens traffic safety [9]. Therefore, cementitious materials such as lime and cement are widely used in the subgrade construction of the YRAP to improve the water stability and durability of the alluvial silt [4].

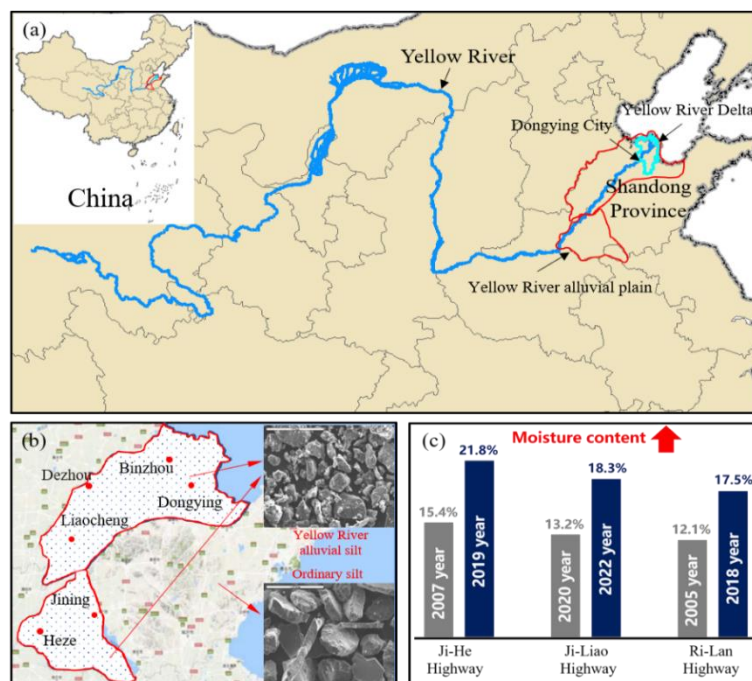


**Figure 1.** (a) The location and area of YRAP, (b) distribution of alluvial silts and (c) subgrade moisture variation of three Highways located in YRAP.

Compared with large-scale soil replacement, the wide use of lime and cement in areas that lack coarse-grained soils for soil improvement can save project investment, and their raw materials are locally available [10–13]. Studies show that lime-improved soil has low early strength, poor water stability and obvious dry-shrinkage cracking, and it is no longer used in high-grade pavement base course [14]. Portland cement is extensively employed in soil improvement (e.g., expansive soil [15], soft soils [16] and dredged sludge [17]). However, the evaporation of water in cement-improved soil will cause significant shrinkage and cracking during construction [14]. At the same time, due to the high-temperature sensitivity of silicate materials, the strength of cement-improved soil decreases sharply during freeze–thaw cycles, and cannot ensure the stability and durability of subgrade structures in seasonally frozen regions [18,19]. Moreover, the production of cement always releases a large amount of carbon dioxide and aggravates environmental pressure [20,21]. Therefore, it is urgent to develop a kind of economic and environmental cementitious material to reduce the use of cement and improve the frost resistance and water stability of improved soil.

Industrial solid waste (ISW) such as steel slag (SS), desulfurization products (DP) and mineral slag (MS), etc., has been used as backfills in all kinds of engineering construction [22–24], but the stability problem caused by the water swelling of the large-scale application of ISW restricts its practical application [25,26]; whereas, it provides an idea for the study of improved silt in subgrade construction [24,27]. A survey shows that the annual output of ISW in China is more than 3 billion tons, including 500 million tons of MS, 120 million tons of desulfurization products (DP) and 100 million tons of SS, which not only takes lots of land and farms for landfill, but also causes the severe pollution of the environment [28]. A mass of ISW resources can be utilized to produce curing agents and improve soil. Therefore, a great deal of work about ISW-improved soil has been carried out

by scholars. Most of the studies focus on curing mechanisms and performance evaluation. Lang et al. (2021) confirmed the good applicability of blast-furnace slag in the solidification of dredged sludge [29]. Mozejko et al. (2020) explored the solidification mechanism of SS-improved silty clay and showed that the alkaline environment generated by SS hydration could promote the occurrence of pozzolanic reactions [30]. Lang et al. (2020) indicated that the addition of SS could significantly enhance the strength of cement-improved dredged sludge [31]. Huang et al. (1994) found that desulfurized gypsum not only enhanced the pozzolanic reaction using sulfate excitation, but also promoted the formation of ettringite expansion to fill pores [32]. Ye et al. (2021) confirmed the soft-soil-stabilized performance of a GS agent was better than cement [33]. Test results showed that the unconfined compressive strength (UCS) of improved soil could reach 4 MPa after 28 days with 16% GS agent; that of the cement improved soil was only 1.73 MPa. Sun et al. (2021) developed a novel composite cementitious material made of blast-furnace slag, fly ash, desulfurized gypsum and cement; it was found that the early strength of improved silt soil was mainly derived from the hydration reaction of cement components, and the later strength was provided by the pozzolanic reaction of ISW components [34].

The above study results can provide important guidance for the research into ISW curing agents. Some results have detailed research on material proportion design and curing mechanisms [35–37], but most of the results are still in the laboratory test stage [29–31,34] and lack application research in practical engineering. Moreover, most of the studies mentioned above focus on improved dredged sludge and soft soils. In fact, the silty soils widely distributed in the YRAP also need to be improved in practical engineering construction. It is worth noting that the heavy industry in the YRAP is very developed, and an annual increase in ISW by about 10 % (i.e., 290 million tons) of the whole country [38]. Therefore, it is necessary to conduct a theoretical exploration and practical demonstration for the consumption of ISW and the application of ISW-improved alluvial silt.

This paper aims to develop a low-cost and environmentally friendly ISW curing agent to reduce or replace the use of cement in alluvial-silt stabilization. Combined with the current construction needs of subgrade engineering in the YRAP, the optimal proportion of ISW curing agent was determined by response surface methodology (RSM). Then, ISW-improved silt and cement-improved silt were subjected to comparative tests (i.e., UCS test, California bearing ratio (CBR) test, water stability (WS) test and wetting–drying (WD) cycles test) for the performance analysis. Scanning electron microscope (SEM) and X-Ray diffraction (XRD) tests were performed for the microstructure characterization and mechanism analysis. Finally, the feasibility of using an ISW curing agent instead of cement for alluvial-silt stabilization was evaluated using an in-situ test. The relative investigation is expected to provide guidance and application popularization for the novel ISW curing agent.

## 2. Materials and Methods

### 2.1. Test Materials

#### 2.1.1. Industrial Solid Waste

Steel slag (SS) is the main composition of developed curing agent, which employs the first-class SS powder from a SS factory in Laiwu city of Shandong province, China. The common treatment method for recycling the Fe in SS is adopted by the SS factory; in addition, f-CaO and f-MgO in SS are disposed and removed with bottom-convection heat-conduction method [36,39]. Specific surface area of the SS is 420–550 m<sup>2</sup>/kg, and the activity index is more than 95%. Table 1 shows the chemical compositions of the SS.

**Table 1.** Chemical composition of materials.

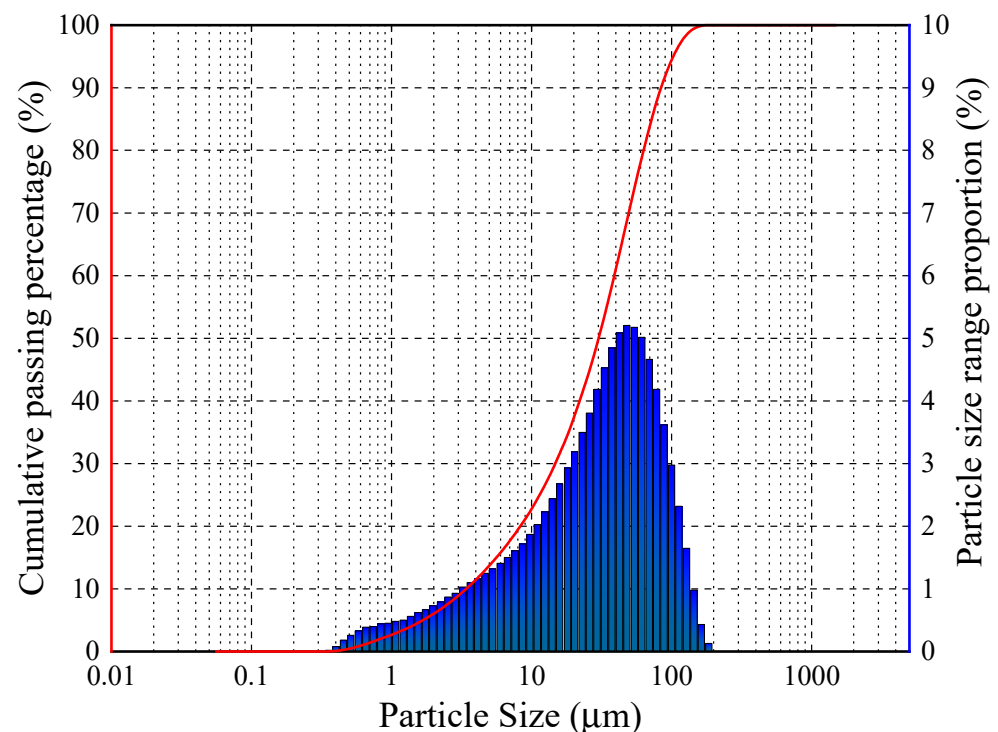
Materials	Chemical Composition (wt%)							
	CaO	SiO <sub>2</sub>	Al <sub>2</sub> O <sub>3</sub>	MgO	Fe <sub>2</sub> O <sub>3</sub>	SO <sub>3</sub>	TiO <sub>2</sub>	K <sub>2</sub> O
SS	30.62	16.28	8.72	6.29	28.57	—	—	—
MS	44.71	29.29	14.85	7.33	0.39	1.28	0.68	0.41
DP A	3.44	49.93	36.17	0.79	5.8	1.12	1.01	1.17
DP B	45.35	1.56	0.8	0.35	0.12	50.63	0.02	0.41
Portland Cement	63.21	18.48	6.74	3.24	3.45	3.16	0.35	—

MS is the industrial solid waste formed in the process of iron making; the MS powder used in this study is the first-class MS of an iron-making plant in Laiwu, Shandong province, China. DP A and B were obtained from a power plant in Ningbo, Zhejiang province. Their chemical compositions are shown in Table 1.

In addition, common Portland cement was employed to be as a control group for comparison test. The compositions of P.O 42.5 Portland cement produced by Shandong Jinan Shanshui Cement Group Co. Ltd. (Jinan, China) are also shown in Table 1.

### 2.1.2. Alluvial Silt

Alluvial silt of the Yellow River was taken from Heze section of Ri-Lan Expressway; the soil specimens were subjected to common geotechnical tests; particle size distribution of soil specimen is shown in Figure 2, and Table 2 presents the basic physical property index of silt. The content of clay grain ( $d < 5 \mu\text{m}$ ), silt grain ( $5 \mu\text{m} < d < 75 \mu\text{m}$ ) and sand grain ( $75 \mu\text{m} < d < 200 \mu\text{m}$ ) were 13.7%, 73.51% and 13.79%, respectively; specimen soil is judged as low liquid limit silt (ML).

**Figure 2.** Particle size distribution of the soil.

**Table 2.** Physical indexes of soil.

Items	Values	Specifications
Natural moisture content (%)	5.9	ASTM D2216-10
Specific gravity	2.69	ASTM D854
Liquid limit (%)	23.5	ASTM D4318
Plastic limit (%)	18.0	ASTM D4318
Plasticity index (%)	5.5	ASTM D4318
Maximum dry density (g/cm <sup>3</sup> )	1.81	ASTM D1557
Optimum moisture content (%)	12.1	ASTM D1557

2.2. Test Methods

2.2.1. Mechanical Test

(i) Unconfined compressive strength (UCS) test

The shapes and dimensions of test samples for compressive strength have no uniform specification worldwide [40,41]. UCS test was conducted according to CN standards JTG E51-2009 *Test Methods of Materials Stabilized with Inorganic Binders for Highway Engineering* [42]. The cylindrical specimen diameter was 50 mm and the height was 50 mm (see Figure 3).

(ii) California bearing ratio (CBR) test

Specimens were subjected to CBR test according to AASHTO T193-13 *Standard Method of Test for The California Bearing Ratio* [43] with YDLQ comprehensive strength tester for pavement materials (see Figure 3).

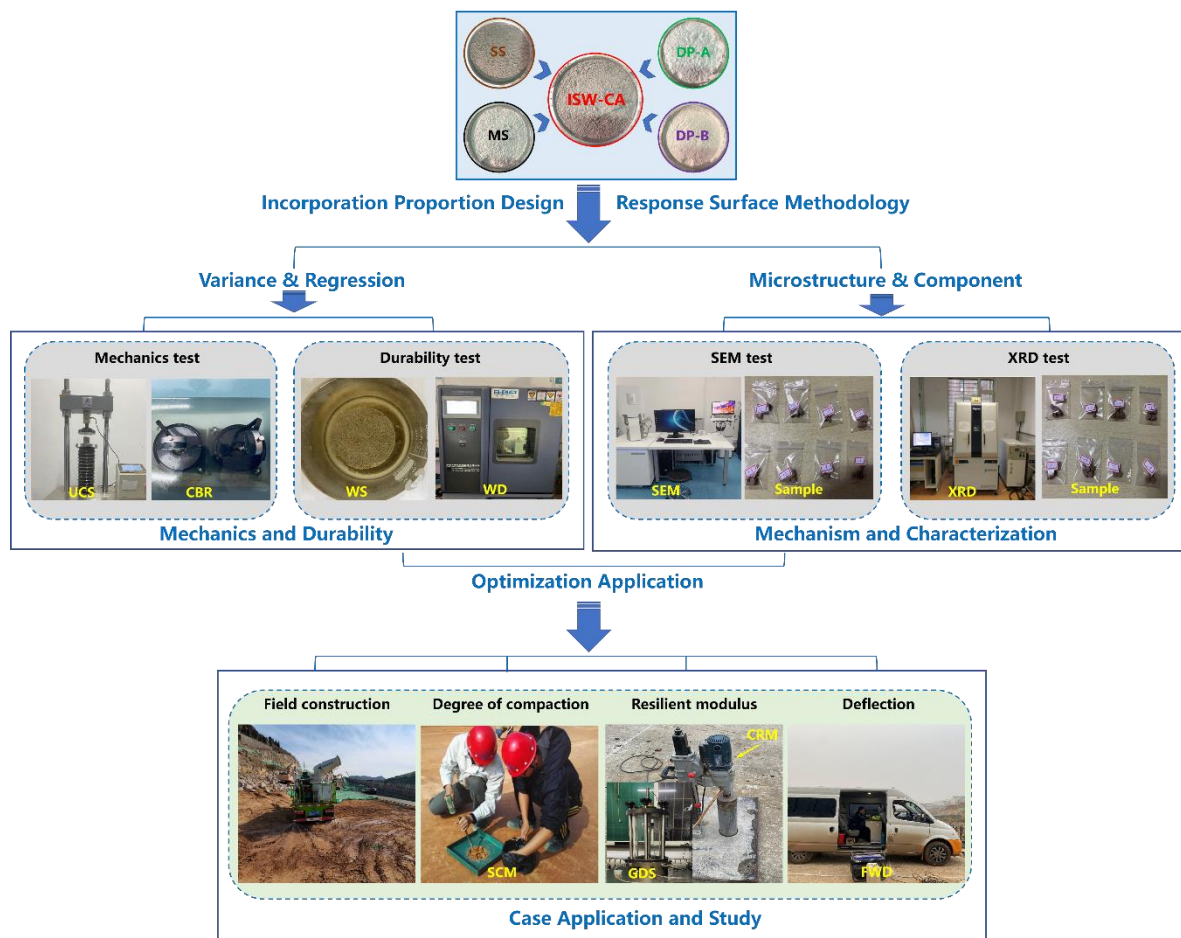


**Figure 3.** Evaluation study flowchart.

### 2.2.2. Durability Test

#### (i) Water stability (WS) test

The specimen size used in water stability test was the same as that of UCS test. Specimen in the last day in specific curing period needed to be immersed into water (i.e., immersion for 24 h, see Figure 3), then it was subjected to UCS test, and WS factor was calculated with the UCS of specimen met corresponding to full curing period according to the Equation (1):

$$K_{WS} = \frac{q_{uw}}{q_{uw0}} \times 100\% \quad (1)$$

where  $K_{WS}$  is the WS factor,  $q_{uw}$  is the UCS of specimen for immersion of 24 h, and  $q_{uw0}$  is the UCS of specimen met corresponding full curing period.

#### (ii) Wetting–drying cycle (WD) test

ASTM D4843-88 standard (2016) provides general guidance for WD cycle test, and improvement and innovation were also made for the detection of WD resistance in specific experiments [44]. In this study, the specimen size used in WD cycle test was the same as that of UCS test. After the specimens met the target curing period, a drying process was first conducted in each WD cycle. The specimens were wrapped with filter paper to achieve the target moisture contents (i.e., 4%). Then, the specimens were subjected to humidifier curing for 24 h with the moisture increment of 1.08 g/h, so that the moisture content reached 20.4% at the end of the wetting process (see Figure 3). The drying and wetting process is a complete W-D cycle [45]. Finally, UCS test was conducted on the specimens, and WD factor was calculated with the UCS of specimen meeting specific number of W-D cycle, according to the Equation (2):

$$K_{WD} = \frac{q_{ud}}{q_{ud0}} \times 100\% \quad (2)$$

where  $K_{WD}$  is the WD factor,  $q_{ud}$  is the UCS of specimen under specific number of W-D cycle, and  $q_{ud0}$  is the UCS of specimen meeting corresponding full curing period.

The average value of duplicates of the fore-mentioned tests for each specimen was taken as the final measured data.

### 2.2.3. Microcosmic Characterization

SEM (Hillsborocity, OR, USA) and XRD (Zeiss Oberkochen, Germany) were employed to characterize microstructure and analyze the action mechanism of improved soil (see Figure 3). Specimen fragments crushed in the previous UCS test could be reused, fragments of about 1 cm<sup>3</sup> were dried under 40 °C and then stored in anhydrous ethanol. Silt powders ground into fragments were subjected to the metal-spraying process for SEM test, and silt powders were subjected to XRD test, exposure time of 1 s per step, sampling step was 0.02°, scanning speed was 2°/min, and scanning range was from 10° to 70°.

### 2.2.4. In-Service Performance

Resilient modulus (AASHTO T 307-99 [46]) is an important indicator to characterize subgrade-soil stiffness and strength. To ensure the accuracy of the comparative test, the resilient modulus was determined by field sampling with dynamic triaxial testing in the laboratory. The degree of compaction and deflection are the quality inspection indexes of subgrade construction. The degree of compaction in subgrade soil was determined by sand replacement method. Falling weight deflectometer (FWD, SHUOGUAN, Shnghai, China) was employed for rapid determination of the deflection of subgrade soil in case study (ASTM D 4695-03 [47]).

## 2.3. Evaluation Schemes

### 2.3.1. Incorporation Proportion Design

Alluvial silt of the Yellow River was taken as the object of improved soil, response surface methodology (RSM) was employed to determine the optimum proportion [48–51]. Central composite design (CCD) was used for the test arrangement; SS, MS, DP-A and

DP-B were taken as the influencing factors; the different incorporation ratio of each material is used as influencing level. UCS of improved soil after 7 days' curing period was regarded as the response value, in the consideration of saving the construction period for in-situ application. There are 4 factors, 16 angle points, 8 axis points, 6 center points, 30 tests in this CCD. Consequently, SS:MS:DP-A:DP-B = 52:20:19:9 was considered as the optimum proportion of ISW-curing-agent-improved soil based on RSM.

### 2.3.2. Test Arrangement for Improved Soil

The improved soil specimens with two kinds of curing agent (cement and ISW) and various curing agents incorporated (2%, 4%, 6%, 8%, 10%) at different curing ages (7 days, 28 days, 90 days, 180 days, 270 days) were subjected to mechanical and durability tests; test results were also statistically analyzed with variance. Incorporation and curing age were considered as factors, whereas UCS, CBR, WS factor and WD factor were chosen as responses. Curing mechanism and microcosmic characterization were further investigated. Finally, in-situ test of subgrade backfill soil service performance was conducted for popularization and application. The whole evaluation study flowchart is shown in Figure 3.

## 3. Analysis of Mechanical and Durability

### 3.1. Mechanical Test Result and Analysis

Figure 4 shows the UCS variation curve of the two kinds of improved silt with the increase in curing-agent incorporation and curing age. It can be seen that the UCS of the two kinds of improved silt grows with the increase in incorporation and curing age and then tends to be stable. The incorporation and curing age are conducive to improve the UCS, but more is not always better for saving costs and the construction period. A strength of 7 days and 28 days show a large proportion of final strength; they are of some instructive significance to evaluate the application of improved silt. The reduction in increase rate is more observable when the incorporation is increased up to 6% and 8%. When the incorporation is increased from 6% to 8%, the UCS of ISW-improved silt under different curing ages is enhanced by 12.62%~20.37%, while the UCS of cement-improved silt under different curing ages is enhanced by 12.38%~15.56%. When the incorporation is increased from 8% to 10%, the UCS of ISW-improved silt under different curing ages is improved by 1.69%~7.69%, while the UCS of cement-improved silt under different curing ages is improved by 3.33%~6.73%. The UCS of ISW-improved silt is more susceptible to curing age. At the same time, note that the UCS of cement-improved silt in early stages is generally higher than that of ISW-improved silt with the same incorporation and curing age.

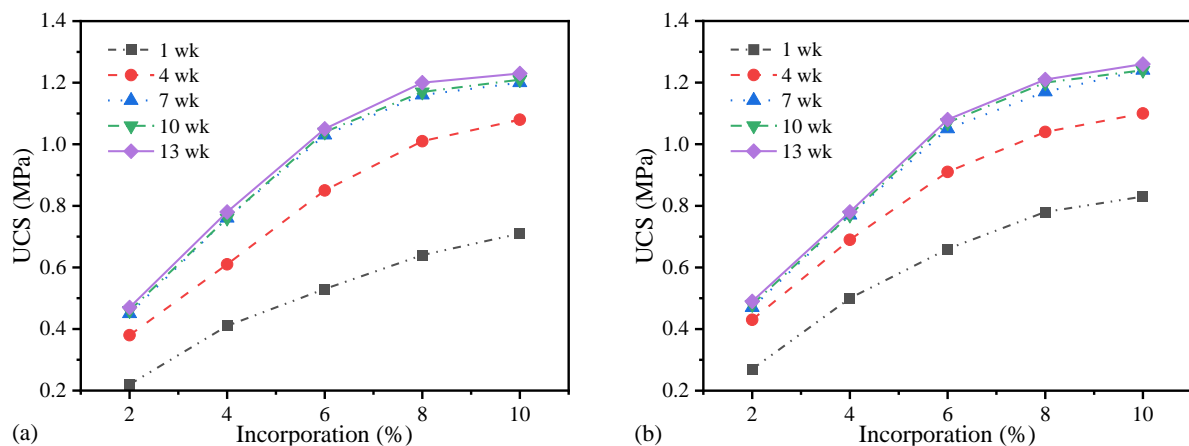


Figure 4. UCS of (a) ISW-improved silt and (b) cement-improved silt.

Improved silt used as the backfill soil for subgrade depends on the compressive strength to evaluate subgrade quality. CBR is another important indicator for the characteri-

zation of subgrade strength. In order to further explore the mechanical properties of the two improved silts, the CBR test was conducted and the results are shown in Figure 5. What can be seen in Figure 5 is that the increase in CBR is significantly affected by the incorporation and curing age. The reduction in increase rate is obviously witnessed when the incorporation is increased up to 8%. When the incorporation is increased from 8% to 10%, the CBR of ISW-improved silt under different curing ages is improved by 6.29%~11.78%, while the CBR of cement-improved silt under different curing ages is improved by 7.31%~10.78%. Similarly, the CBR of ISW-improved silt in the early stage is generally lower than that of cement-improved silt and is more susceptible to curing age, while it fully conforms to the requirements of the minimum CBR of subgrade backfill [52]. From the results of the UCS and CBR test, there is not much difference in strength of the two improved silts with adequate curing.

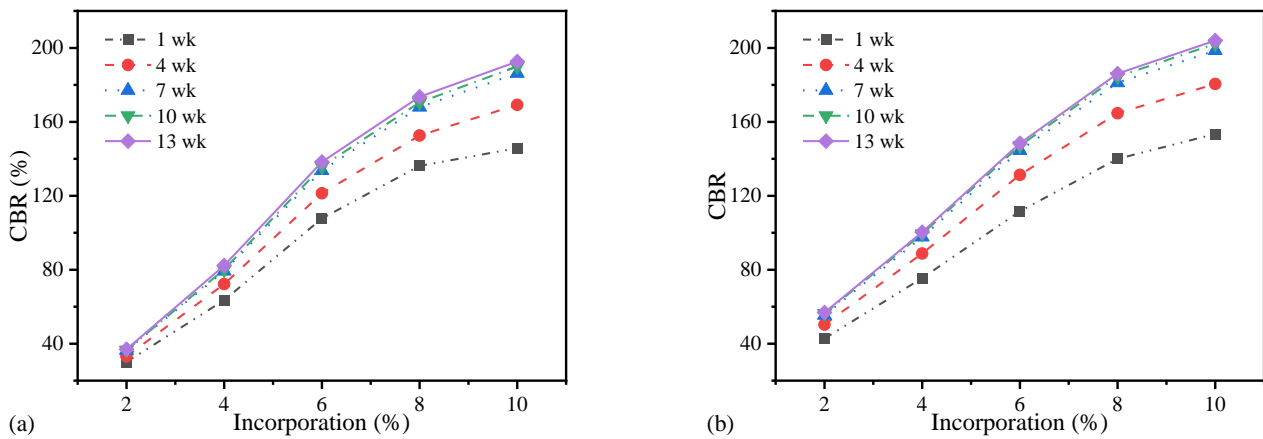


Figure 5. CBR of (a) ISW-improved silt and (b) cement-improved silt.

3.2. Durability Test Result and Analysis

Figure 6 depicts the water-stability variation of the two kinds of improved silt with incorporation. When the incorporation is increased from 2% to 10%, the WS factor of ISW-improved silt under different curing ages is improved by 47.73%~100%, while the WS factor of cement-improved silt under different curing ages is improved by 47.92%~90.32%. When the curing age is increased from 1 week to 13 weeks, the WS factor of ISW-improved silt under different incorporations is improved by 31.56%~70.37%, while the WS factor of cement-improved silt under different incorporations is improved by 25.42%~61.29%. Simultaneously, note that the amplification of WS factor with identical curing periods (from 1 week to 13 weeks) declines with the increase in incorporation. Blindly increasing the addition cannot make the curing agent act with high efficiency.

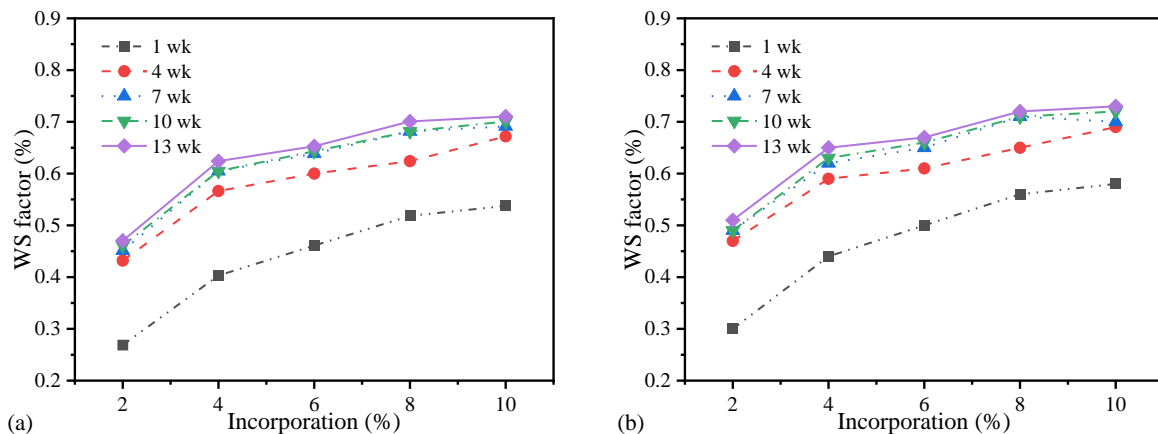


Figure 6. WS factor of (a) ISW-improved silt and (b) cement-improved silt.

WD cycles could deteriorate soil microstructure and incur strength heterogeneity. Study on the WD factor is beneficial to explore the durability of improved silt from another expective. The two kinds of improved silt were subjected to the WD cycle test; the results are exhibited in Figure 7 (specimens with some incorporation that could not withstand three WD cycles are not exhibited).

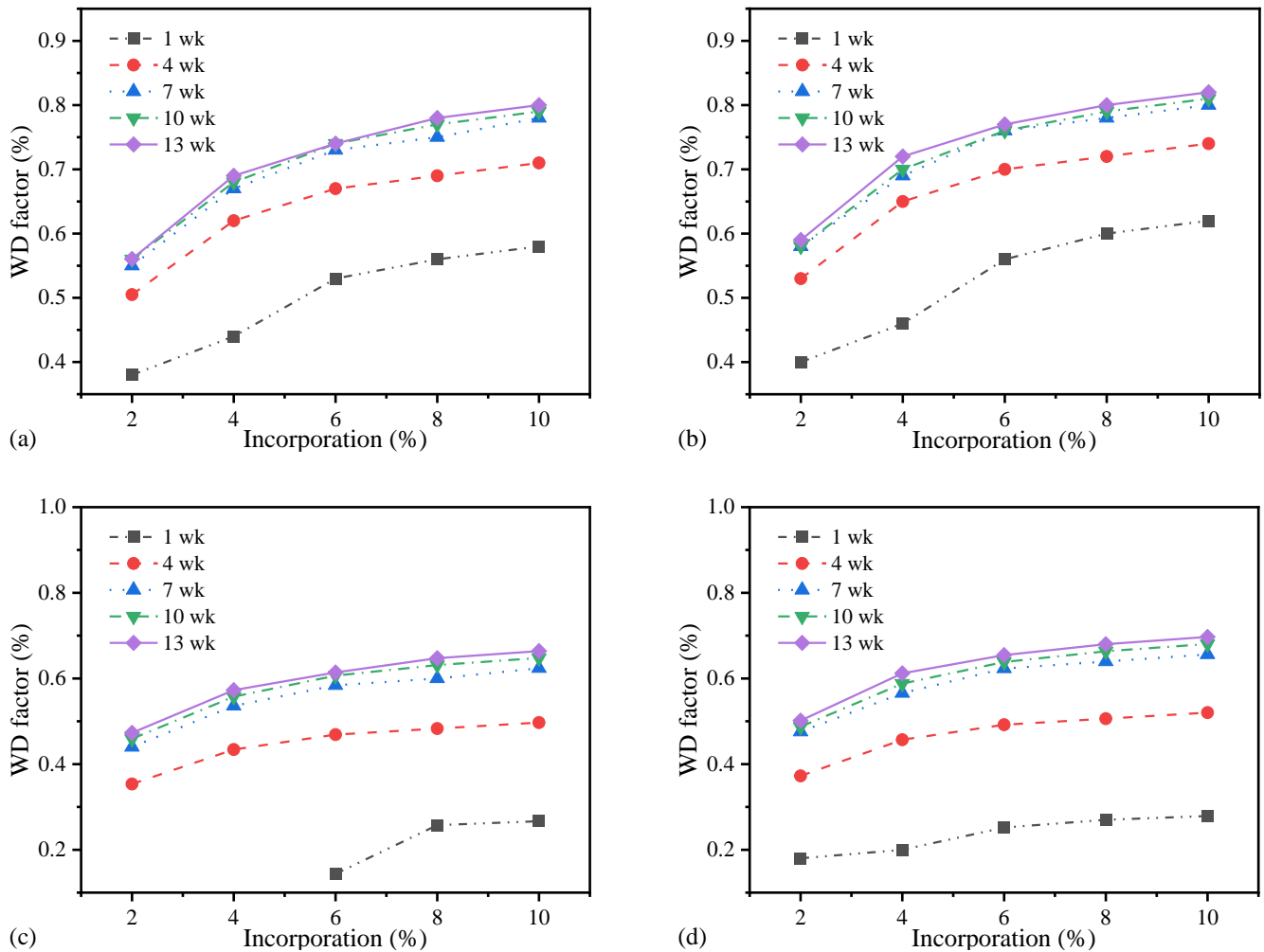


Figure 7. Wetting–drying stability of ISW-improved silt under (a) 1 WD cycle and (c) 3 WD cycle; cement-improved silt under (b) 1 WD and (d) 3 WD cycle.

As can be observed from Figure 7, when the incorporation is increased from 2% to 10%, the WD factor of ISW-improved silt under different curing ages and 1 WD cycle is improved by 40.35%~59.46%, while the WD factor of cement-improved silt under different curing ages and 1 WD cycle is improved by 39.66%~61.54%. When the curing age is increased from 1 week to 13 weeks, the WS factor of ISW-improved silt under different incorporation and 1 WD cycle is improved by 35.59%~60.47%, while the WD factor of cement-improved silt under different incorporation is improved by 28.57%~60.00%. It can be inferred that the WD factor improvement of ISW-improved silt under 1 WD cycle is more stable than that of cement-improved silt. ISW-improved silt specimen with curing age of 7 days and little incorporation cannot withstand three WD cycles, while the WD factor of the cement-improved silt specimen can be obtained under same conditions. This indicates that cement helps in enhancing the early strength is more obvious than that of the ISW curing agent. Both of the two kinds of improved silt can meet the requirements of durability. To sum up, ISW-improved silt can present good mechanical and durability with good curing condition and curing age, and is expected to replace the cement-improved silt.

### 3.3. Statistical Analysis for ISW-Improved Silt

The mechanical and durability properties of ISW-improved silt were further analyzed and validated using general factorial design. Different incorporation of the ISW curing agent and curing age were chosen as factors, while UCS, CBR, WS factors and WD factor (one WD cycle) were considered as responses. Variance analysis and multiple regression analysis were used to analyze the effect of factors on responses statistically and to check the significance and correlation of suggested models; the variance analysis model is established and the analysis results are shown in Table 3.

**Table 3.** The results of variance analysis.

Source	Items	Sum of Squares	Df	Mean of Squares	F Value	p Value	Significance
Model	UCS	4.81	24	0.2005	4575.20	<0.0001	Significant
	CBR	$1.458 \times 10^5$		6075.29	7694.03	<0.0001	Significant
	WS factor	0.6440		0.0268	879.50	<0.0001	Significant
	WD factor	0.6608		0.0275	1119.90	<0.0001	Significant
A	UCS	3.34	4	0.8355	19,061.91	<0.0001	-
	CBR	$1.390 \times 10^5$		34,747.06	44,005.27	<0.0001	-
	WS factor	0.3799		0.0950	3113.18	<0.0001	-
	WD factor	0.3230		0.0807	3284.13	<0.0001	-
B	UCS	1.37	4	0.3425	7813.16	<0.0001	-
	CBR	5425.74		1356.44	1717.85	<0.0001	-
	WS factor	0.2607		0.0652	2135.78	<0.0001	-
	WD factor	0.3333		0.0833	3389.42	<0.0001	-
AB	UCS	0.1010	16	0.0063	144.03	<0.0001	-
	CBR	1393.04		87.06	110.26	<0.0001	-
	WS factor	0.0034		0.0002	7.01	<0.0001	-
	WD factor	0.0045		0.0003	11.46	<0.0001	-
Residual	UCS	0.0011	24	0.0000	-	-	-
	CBR	18.95		0.7896	-	-	-
	WS factor	0.0007		0.0000	-	-	-
	WD factor	0.0006		0.0000	-	-	-
Cor total	UCS	4.81	49	-	-	-	-
	CBR	$1.458 \times 10^5$		-	-	-	-
	WS factor	0.6448		-	-	-	-
	WD factor	0.6618		-	-	-	-

As can be seen from Table 3, the UCS, CBR, WS factor and WD factor model are furnished with a high  $F$  value and low  $p$  value which is less than 0.05; it indicates that the models are significant. In addition, the positive probability distribution of model residual of each model is depicted in Figure 8. What can be seen is that most test points are evenly distributed in and near the straight line. It indicates that the residuals of UCS, CBR, WS factor and WD factors are independent of the predictive variables, and conform to normal distribution with fewer outliers. It can be considered that incorporation and curing age have good adaptability to the UCS, CBR, WS factor and WD factor model.

Figure 9 presents the predicted value and test value distribution of the UCS, CBR, WS factor and WD factor model. Most of the test points are on the line of  $y = x$ , which means that the predicted value is basically close to the actual value, and the established model is reasonable. The quadratic fit model as shown in Equation (3) was employed for the regression analysis.

$$Y = X_0 + X_1A + X_2B + X_3A^2 + X_4B^2 + X_5A \times B \quad (3)$$

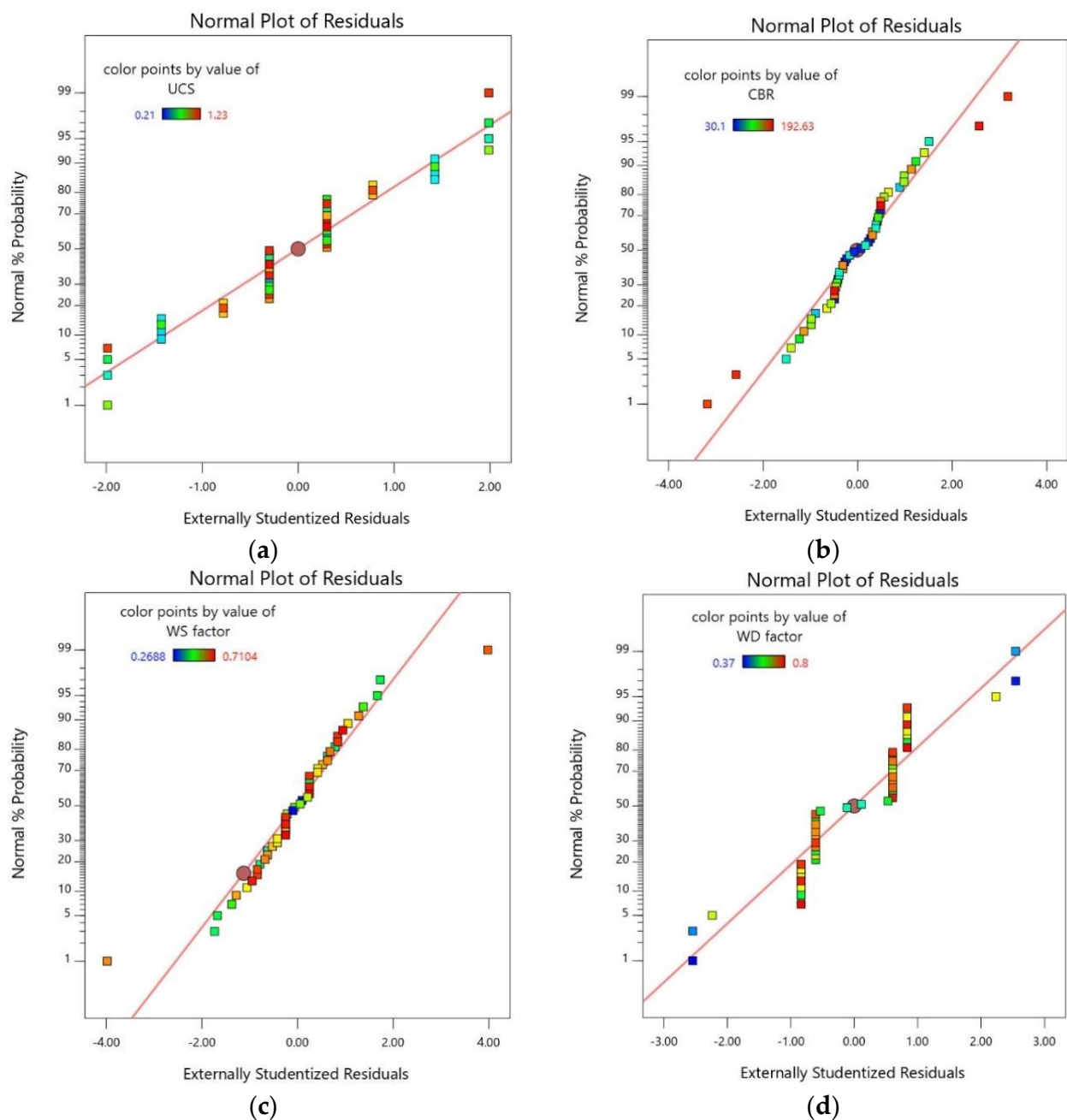


**Figure 8.** Positive probability distribution of (a) UCS model residual, (b) CBR model residual, (c) WS factor model residual and (d) WD factor model residual.

The fit statistics are presented in Table 4, which shows the factors are consistent with responses in each model.  $R^2$  represents the degree of fitness and quality of developed models; that the value of  $R^2$  is larger than 0.95 shows the corresponding model is well-fitted and indicates significant agreement between actual and predicted responses. In addition, the numerical difference between it and adjusted  $R^2$  is less than 0.2, demonstrating that the established models are of significance in predicting the responses. The selected models are well-fitted and highly significant and can be used to establish a correlation between factors and responses; the three-dimensional diagrams are shown in Figure 10.

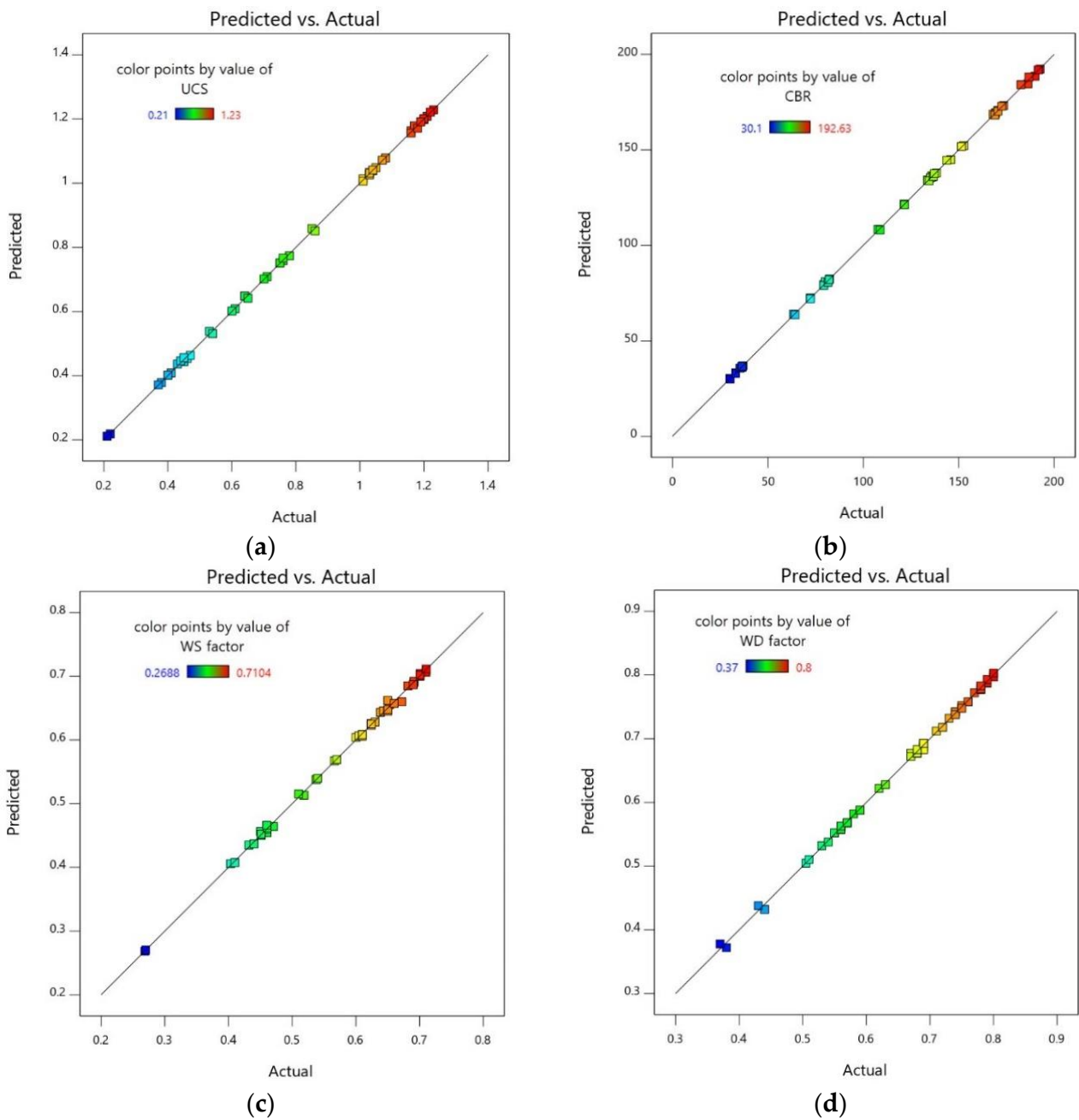


**Figure 9.** Distribution of (a) UCS predicted value and test value, (b) CBR predicted value and test value, (c) WS factor predicted value and test value, (d) WD factor predicted value and test value.

**Table 4.** The results of variance analysis.

Model	X <sub>0</sub>	X <sub>1</sub>	X <sub>2</sub>	X <sub>3</sub>	X <sub>4</sub>	X <sub>5</sub>	R <sup>2</sup>	Adj. R <sup>2</sup>
UCS	−0.2695	0.1841	0.0917	−0.0096	−0.0052	0.0026	0.9825	0.9779
CBR	−36.4012	30.1130	3.3160	−1.2070	−0.2449	0.4026	0.9922	0.9901
WD factor	0.2049	0.0692	0.0500	−0.0037	−0.0025	+2.8 × 10 <sup>−4</sup>	0.9824	0.9777
WS factor	0.1015	0.0825	0.0477	−0.0043	−0.0023	−2.88 × 10 <sup>−4</sup>	0.9588	0.9480

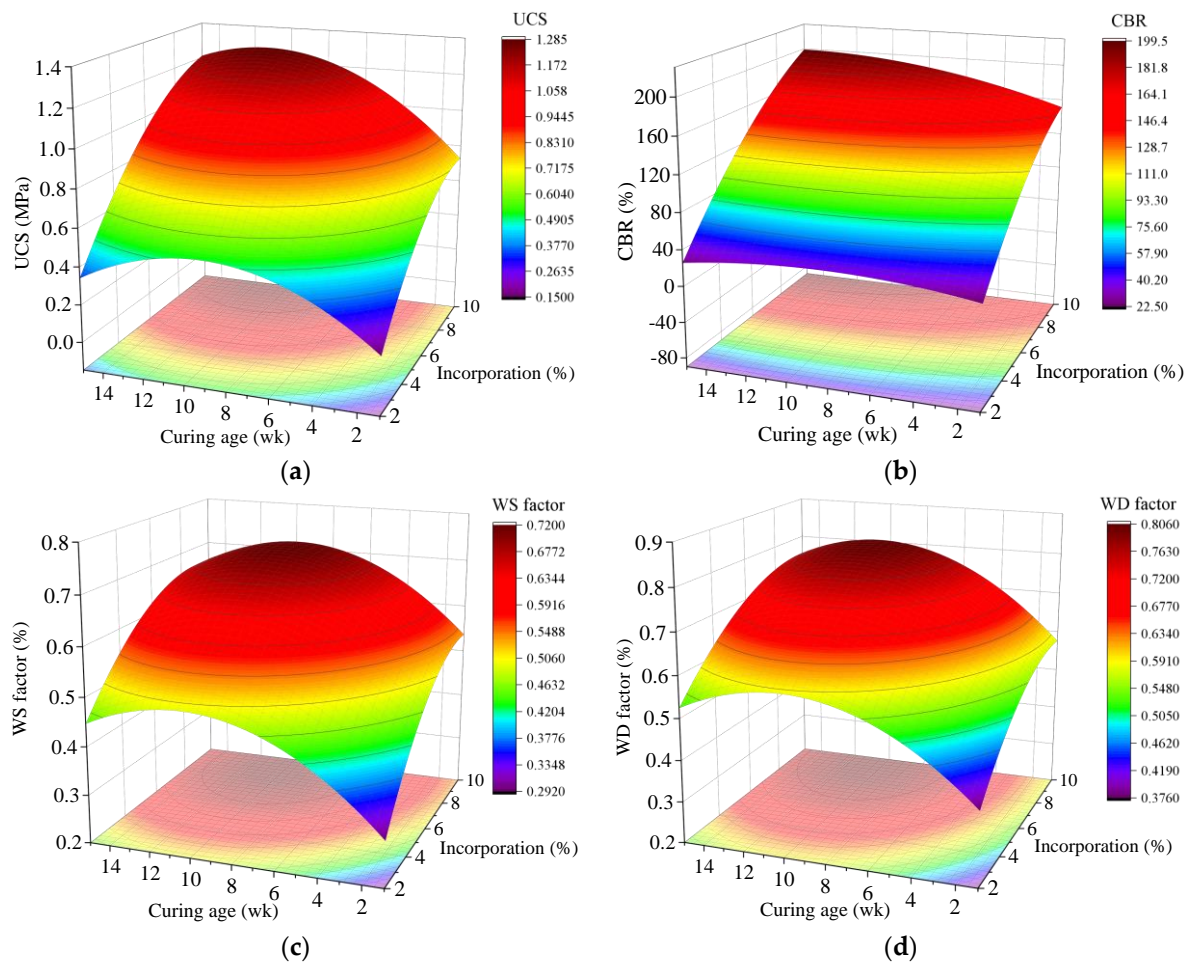


**Figure 10.** Effect of incorporation and curing age on (a) UCS, (b) CBR, (c) WS factor and (d) WD factor.

## 4. Discussion

### 4.1. Scanning Electron Microscope Analysis

Figure 11 depicts the microstructure morphology of ISW-improved silt and cement-improved silt with different curing agents incorporation and curing age. The addition of a curing agent strengthens the cation exchange on the silt-particle surface and promotes the agglomeration of particles [53]. A large number of hydration products are attached to the particles of improved silt; floc or reticulate Calcium silicate hydrate (C-S-H), and needle-shaped or rod-shaped Ettringite (Aft) can be observed in ISW-improved silt with a 7 d curing age (Figure 11a). There may be a synergism between the four ISW materials; the MS and DP B in the ISW curing agent are activated in the alkaline environment and the calcium aluminate hydrate (C-A-H) is converted into Aft. However, there is C-S-H attaching to the cement-improved silt particle; Aft is hard to see in Figure 11b, which is consistent with cement hydration mechanisms. In addition, vast quantities of pores between soil particles can be observed in both of the two improved silts with 7 days curing age.

As can be seen in Figure 11c,d, many C-S-H and Aft are further produced with the increase in curing age; soil particles are connected and filled by these hydration products and soil strength is enhanced in this way [54,55]. Figure 11d indicates that dicalcium silicate in cement-improved silt is converted to C-S-H; the pore feature between soil particles is not obvious. When the reaction goes further, the production of C-A-H, which is hard to observe, is combined with the sulfate of the DP and forms Aft. The interlaced growth in Aft with C-S-H leads to tighter connections for silt particles. The pores of the two improved silts with 28-day curing age are almost identical, indirectly indicating the fact that the UCS of the two improved silts with 28 days curing age are almost same. The mechanical

performance is attributed to the spatial reticular structures formed by the curing agent in the improved soil [33].

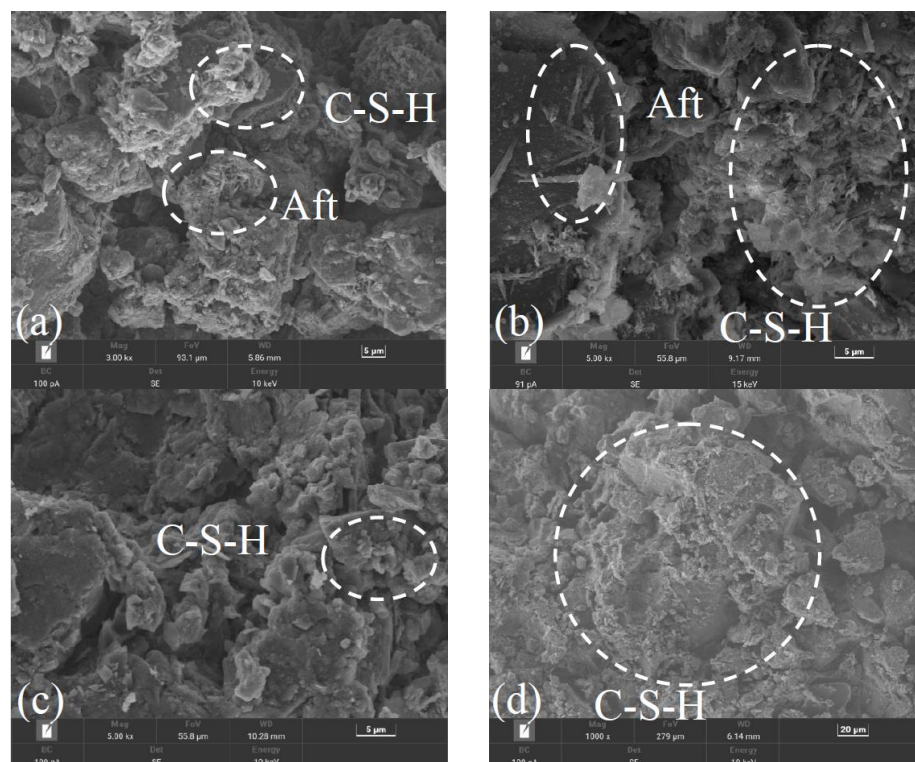
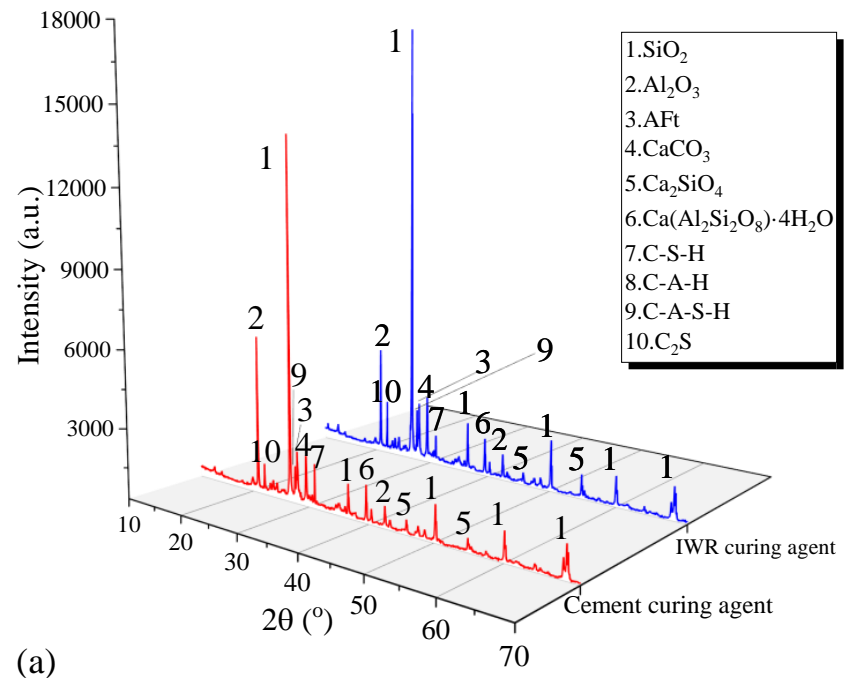


**Figure 11.** SEM pattern of ISW-improved silt with (a) curing age of 7 days and (b) curing age of 28 days, cement-improved silt with (c) curing age of 7 days and (d) curing age of 28 days.

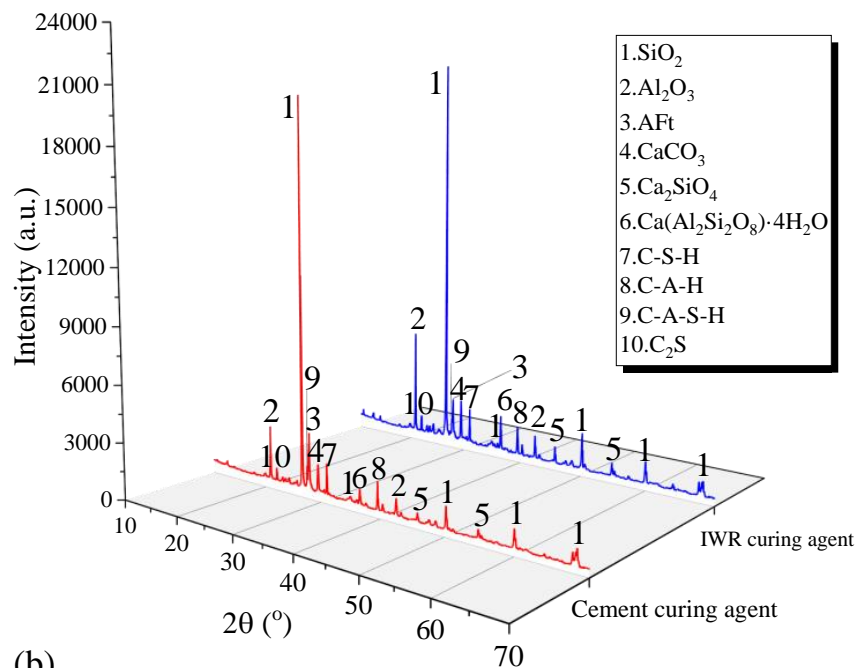
#### 4.2. X-ray Diffraction Analysis

XRD patterns of different improved silt are shown in Figure 12, at  $2\theta = 26.2^\circ$ , there is obvious diffraction peak of  $\text{SiO}_2$ , which is mainly from silt particles. The diffraction peak of C-S-H, C-A-H, C-A-S-H and Aft in the two kinds of improved silt with the curing age of 7 days can be observed in Figure 12a. It indicates the two improved silts produce similar hydration products, while the diffraction peak of Aft shown in ISW-improved silt is higher than that of cement-improved silt; the diffraction peak of C-S-H shown in ISW-improved silt is lower than that of cement-improved silt.  $\text{C}_2\text{S}$  and  $\text{C}_3\text{S}$  in SS and DP can produce C-S-H and  $\text{Ca}(\text{OH})_2$  during the early stage,  $\text{Al}_2\text{O}_3$  in SS can produce C-A-H by hydration, which creates an alkaline environment [29]. The chemical bond of  $[\text{AlO}_4]$  tetrahedron in MS is broken, and the synergistic hydration with  $\text{CaSO}_4$  in DP produces Aft.

As can be seen in Figure 12b, the diffraction peak of hydration products in the two kinds of improved silts with a curing age of 28 days rises; the active substances react with each other further. The hydration and pozzolanic reaction consume quantities of  $\text{Al}_2\text{O}_3$  and  $\text{C}_2\text{S}$ , and produce C-A-H, Aft and C-S-H, which is conducive to connect soil particles and enhance the strength of soil are produced [56–58]. Note that the C-S-H content in ISW-improved silt is slightly lower than that of cement-improved silt; Aft content is slightly higher than that of cement-improved silt. This is due to dicalcium silicate gradually participating in the reaction with curing age, and the reaction rate of ISW is gradually higher than that of cement. It is also confirmed that the strength enhancement amplitude of ISW-improved silt between curing age of 7 days to 28 days is larger than that of cement-improved silt; the difference of hydration products between the two is caused by the difference of their composition.



(a)



(b)

**Figure 12.** XRD diffraction pattern of improved silt (a) at curing age of 7 days, (b) at curing age of 28 days.

### 5. Case Application and Study

#### 5.1. Engineering Situation

It is of practical guiding significance to examine the in-service performance of improved soil in specific applications. In this study, the in-situ test site (K55 + 700~K55 + 900) was chosen from the Heze section of the Ri-Lan Expressway, which is the same site as the specimens sampling site of the laboratory tests. The whole test section is divided into four 50 m test sections (section A, section B, section C and section D, as shown in Figure 13). The degree of compaction, resilient modulus and deflection were tested at specific points (i.e., different curing ages, different locations, different incorporation of ISW curing agent

and cement, as shown in Table 5), respectively. It is worth noting that the results of 48 sets of degree of compaction filed tests all met the construction quality requirements. Therefore, the field data is scientific and reliable in this study.

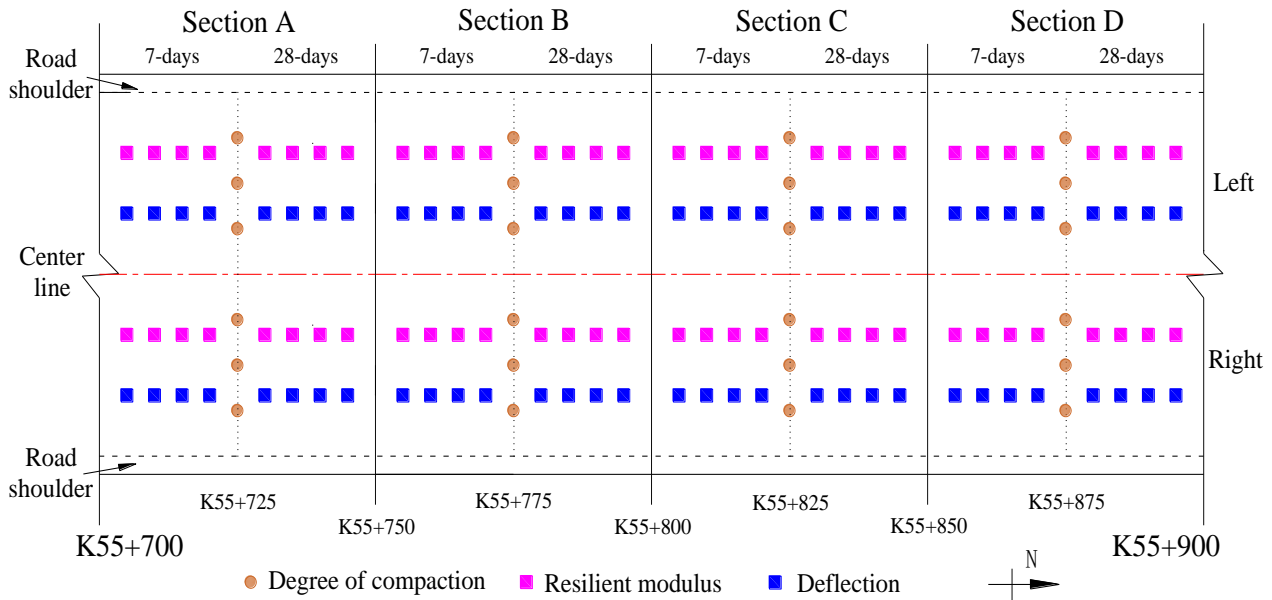


Figure 13. Schematic diagram of the location of in-situ tests.

Table 5. Test cases of degree of compaction, resilient modulus and deflection.

Test Area	Material	Incorporation	Test Point	Curing Age	Locations
Section A	Cement curing agent	4%	Left: 4,4,3	7 days	K55+700~K55+725
			Right: 4,4,3	28 days	K55+725~K55+750
Section B	ISW curing agent	4%	Left: 4,4,3	7 days	K55+750~K55+775
			Right: 4,4,3	28 days	K55+775~K55+800
Section C	Cement curing agent	6%	Left: 4,4,3	7 days	K55+800~K55+825
			Right: 4,4,3	28 days	K55+825~K55+850
Section D	ISW curing agent	6%	Left: 4,4,3	7 days	K55+850~K55+875
			Right: 4,4,3	28 days	K55+875~K55+900

### 5.2. In-Service Performance Analysis

The comparison of the resilient modulus of the two kinds of improved silt is shown in Figure 14. It can be observed that the resilient modulus grows with the increase in incorporation and curing age. With the same curing age, when the incorporation increases from 4% to 6%, the resilient modulus enhancement amplitude of ISW-improved silt is 18.10%~24.42%, which is larger than that of cement-improved silt (15.64%~17.28%). With the same incorporation, when the curing age increases from 7 days to 28 days, the resilient modulus enhancement amplitude of ISW-improved silt is 10.93%~16.86%, which is also larger than that of cement-improved silt (9.36%~10.92%). Though the resilient modulus of ISW-improved silt is slightly less than that of cement-improved silt under the same curing age and incorporation, the resilient modulus enhancement amplitude of ISW-improved silt is larger.

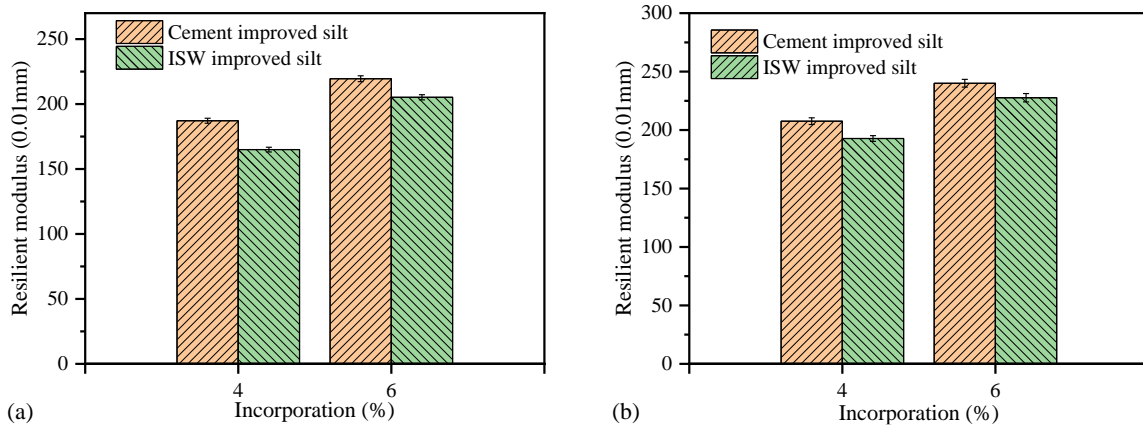


Figure 14. Resilient modulus with (a) curing age of 7 days and (b) curing age of 28 days.

The comparison of the deflection of two kinds of improved silt is shown in Figure 15. It can be seen that the deflection declines with the increase in incorporation and curing age, which indicates the quality of subgrade has been effectively promoted. With the same curing age, when the incorporation increases from 4% to 6%, the deflection reduction amplitude of ISW-improved silt is 19.15%~19.22%, which is less than that of cement-improved silt (26.21%~26.37%). With the same incorporation, when the curing age increases from 7 days to 28 days, the deflection reduction amplitude of ISW-improved silt is 61.00%~61.04%, which is less than that of cement-improved silt (61.84%~61.92%). There is no doubt that the influence of curing age on deflection is more sensitive than incorporation; improved silt with a curing age of 28 days displays greater deformation-resistance behaviors compared to that with a curing age of 7 days. The in-service performance of ISW-improved silt shows little difference to that of cement-improved silt; both of them meet the requirements from the aspect of in-situ application.

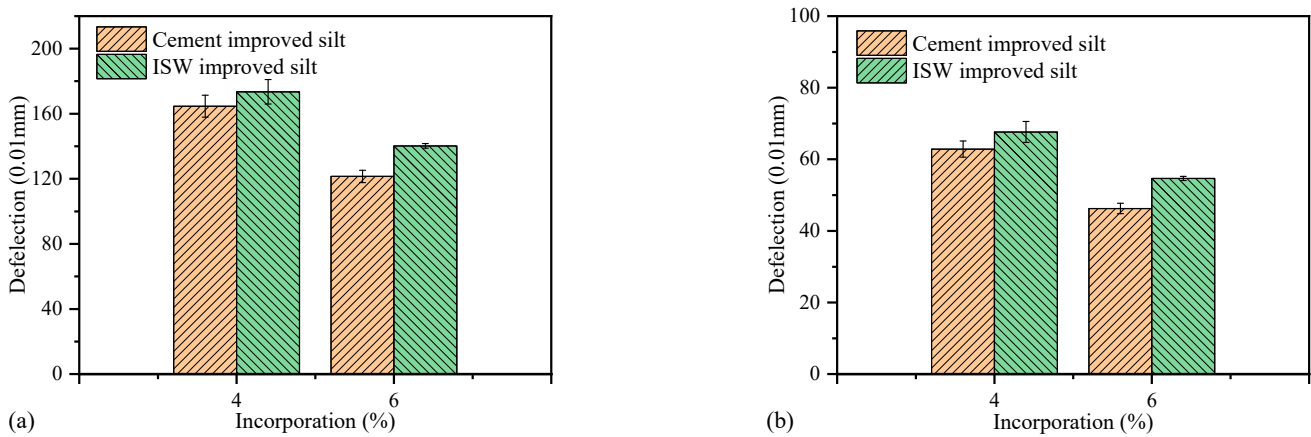


Figure 15. Deflection with (a) curing age of 7 days and (b) curing age of 28 days.

### 5.3. Benefit and Environment Evaluation

Table 6 shows the statistical results of the unit price of curing-agent raw materials. In practice, few costs of industrial waste raw materials are needed when the supply requirement is large enough, and the processing and transportation account for a large proportion of the costs. It can be seen from Table 6 that the unit cost of the ISW curing agent is less than 1/5 that of cement. It will bring great economic benefit to the construction of subgrade, ground and slope treatment.

**Table 6.** Unit price of curing-agent raw materials.

Materials	SS	MS	DP A	DP B	ISW Curing Agent	Cement
Price (CNY/t)	75	350	35	65	121	650

The in-situ test section is taken as an example to evaluate the economic benefit of ISW-improved silt in actual construction. The road width of the test section is 40 m and the length is 50 m; the thickness of improved silt replacement is 0.2 m. The test-section cost is listed in Table 7. It can be estimated that the consumption of ISW curing agent in 4% improved silt is about 5554 t/ km; that in 6% improved silt is about 8172 t/ km.

**Table 7.** Cost comparison of raw materials in the test area.

Test Area	Materials	Incorporation (%)	The Total Amount (t)	Cost (CNY)
Section A	Cement curing agent	4	262.9	170,885.0
Section B	ISW curing agent	4	277.7	33,629.5
Section C	Cement curing agent	6	408.6	265,590.0
Section D	ISW curing agent	6	389.1	47,120.0

It is worth noting that the heavy industry in the YRAP is very developed, and the annual increase in ISW is about 290 million tons, about 140 million tons of SS, 70 million tons of MS and 80 million tons of DP. A large amount of ISW accumulation leads to serious environmental pollution, and the storage of ISW leads to the occupation of plenty of land. Not only does the ISW-improved silt save a lot of construction cost, but also ISW resources are effectively and legitimately utilized. It avoids the environmental pollution caused by the improper treatment of ISW material and has extremely important social significance.

## 6. Conclusions

The comparative tests of ISW-improved silt and cement-improved silt were conducted. Then, the mechanics and durability were analyzed, and the microstructure and action mechanism were characterized. Finally, the feasibility of an ISW curing agent instead of cement was evaluated through in-situ tests. The main conclusions are as follows:

- (i) The UCS, CBR, WS factor and WD factor of the two kinds of improved silt grow with the increase in incorporation and curing age. ISW-improved silt can present good mechanical property and durability, but much weaker than cement-improved silt in the early curing stage. The selected models of variance and regression are highly significant and well fitted; the correlation between factors and responses is established with good agreement.
- (ii) Synergisms in the ISW curing agent are stimulated in the alkaline environment; the interlaced growth in Aft with C-S-H fills the pores between silt particles leads the tighter connection for silt particles. The dicalcium silicate gradually participates in the reaction with curing age and leads the strength-enhancement amplitude of ISW-improved silt between curing ages of 7 days to 28 days to be larger than that of cement-improved silt.
- (iii) The in-service performance of ISW-improved silt has little difference with that of cement-improved silt; both of them meet the requirements from the aspect of in-situ application. The unit cost of the ISW curing agent is less than 1/5 that of cement. A total of 6% incorporation of the ISW curing agent is recommended for the ideal in-service performance and economy. The ISW-improved silt saves a lot of construction cost, and effectively and legitimately utilizes ISW resources. It has extremely important environmental and social significance.

**Author Contributions:** Q.S.: methodology, writing—original draft, validation, funding acquisition. P.J.: methodology, conceptualization, writing—review and editing. X.Z.: supervision, project administration. H.S. (Hao Sun): formal analysis, validation. Y.Y.: formal analysis, writing—review and editing. S.W.: formal analysis. L.L.: validation, writing—review and editing. H.S. (Hongfa Shang): validation. All authors have read and agreed to the published version of the manuscript.

**Funding:** This research was funded by the Natural Science Foundations of China (grant Nos. 52027813, 52178429, and 51778346), and Natural Science Foundations of Shandong Province, China (grant No. ZR2020ME242).

**Institutional Review Board Statement:** Not applicable.

**Informed Consent Statement:** Not applicable.

**Data Availability Statement:** The data presented in this study are available on request from the corresponding author.

**Acknowledgments:** The authors wish to express their sincere gratitude for the support of the Shandong Hi-Speed Group Co., Ltd. and Shandong University.

**Conflicts of Interest:** The authors declare no conflict of interest.

## References

1. Liu, Y.; Liu, J.; Xia, X.; Bi, H.; Huang, H.; Ding, R.; Zhao, L. Land subsidence of the Yellow River Delta in China driven by river sediment compaction. *Sci. Total Environ.* **2020**, *750*, 142165. [[CrossRef](#)] [[PubMed](#)]
2. Zhang, Y.; Feng, X.; Ding, C.; Liu, Y.; Liu, T. Study of cone penetration rate effects in the Yellow River Delta silty soils with different clay contents and state parameters. *Ocean Eng.* **2022**, *250*, 110982. [[CrossRef](#)]
3. Zhang, H.; Sun, Y.; Zhang, W.; Song, Z.; Ding, Z.; Zhang, X. Comprehensive evaluation of the eco-environmental vulnerability in the Yellow River Delta wetland. *Ecol. Indic.* **2021**, *125*, 107514. [[CrossRef](#)]
4. Yao, Z.; Jiang, H.; Sun, M.; Yang, C.; Bao, J.; Cao, R. Analysis of equilibrium density state of highway subgrade with fine soils, China. *J. Highw. Transp.* **2020**, *33*, 94–103. [[CrossRef](#)]
5. Li, K.; Li, Q.; Geng, Y.; Liu, C. An evaluation of the effects of microstructural characteristics and frost heave on the remediation of saline-alkali soils in the Yellow River Delta, China. *Land Degrad. Dev.* **2021**, *32*, 1325–1337. [[CrossRef](#)]
6. Hao, J.; Cui, X.; Qi, H.; Zheng, Y.; Bao, Z. Dynamic behavior of thawed saturated saline silt subjected to freeze-thaw cycles. *Cold Reg. Sci. Technol.* **2022**, *194*, 103464. [[CrossRef](#)]
7. Yao, Y.-P.; Wang, L. Double pot cover effect in unsaturated soils. *Acta Geotech.* **2019**, *14*, 1037–1047. [[CrossRef](#)]
8. Zhang, S.; Teng, J.; He, Z.; Liu, Y.; Liang, S.; Yao, Y.; Sheng, D. Canopy effect caused by vapour transfer in covered freezing soils. *Géotechnique* **2016**, *66*, 927–940. [[CrossRef](#)]
9. Zhang, J.; Hu, T.; Gan, X. Correlation analysis between subgrade performance and pavement disease during operation period. *J. China Foreign Highw.* **2013**, *33*, 12–14. [[CrossRef](#)]
10. Lu, Y.; Liu, S.; Zhang, Y.; Li, Z.; Xu, L. Freeze-thaw performance of a cement-treated expansive soil. *Cold Reg. Sci. Technol.* **2020**, *170*, 102926. [[CrossRef](#)]
11. Nguyen, T.T.H.; Cui, Y.-J.; Ferber, V.; Herrier, G.; Ozturk, T.; Plier, F.; Puiatti, D.; Salager, S.; Tang, A.M. Effect of freeze-thaw cycles on mechanical strength of lime-treated fine-grained soils. *Transp. Geotech.* **2019**, *21*, 100281. [[CrossRef](#)]
12. Tao, Z.; Zhang, Y.; Chen, X.; Gu, X. Effects of freeze-thaw cycles on the mechanical properties of cement-fiber composite treated silty clay. *Constr. Build. Mater.* **2022**, *316*, 125867. [[CrossRef](#)]
13. Bozbeý, I.; Kelesoglu, M.K.; Demir, B.; Komut, M.; Comez, S.; Ozturk, T.; Mert, A.; Ocal, K.; Oztoprak, S. Effects of soil pulverization level on resilient modulus and freeze and thaw resistance of a lime stabilized clay. *Cold Reg. Sci. Technol.* **2018**, *151*, 323–334. [[CrossRef](#)]
14. Wang, S.; Xue, Q.; Zhu, Y.; Li, G.; Wu, Z.; Zhao, K. Experimental study on material ratio and strength performance of geopolymer-improved soil. *Constr. Build. Mater.* **2021**, *267*, 120469. [[CrossRef](#)]
15. Ding, L.-Q.; Vanapalli, S.K.; Zou, W.-L.; Han, Z.; Wang, X.-Q. Freeze-thaw and wetting-drying effects on the hydromechanical behavior of a stabilized expansive soil. *Constr. Build. Mater.* **2021**, *275*, 122162. [[CrossRef](#)]
16. Prakash, K.G.; Krishnamoorthy, A. Stability of Embankment Constructed on Soft Soil Treated with Soil–Cement Columns. *Transp. Infrastruct. Geotechnol.* **2022**. [[CrossRef](#)]
17. Bian, X.; Wang, Z.-F.; Ding, G.-Q.; Cao, Y.-P. Compressibility of cemented dredged clay at high water content with super-absorbent polymer. *Eng. Geol.* **2016**, *208*, 198–205. [[CrossRef](#)]
18. Shibi, T.; Kamei, T. Effect of freeze–thaw cycles on the strength and physical properties of cement-stabilised soil containing recycled bassanite and coal ash. *Cold Reg. Sci. Technol.* **2014**, *106–107*, 36–45. [[CrossRef](#)]
19. Lake, C.B.; Yousif, M.A.-M.; Jamshidi, R.J. Examining freeze/thaw effects on performance and morphology of a lightly cemented soil. *Cold Reg. Sci. Technol.* **2017**, *134*, 33–44. [[CrossRef](#)]

20. Yang, K.-H.; Jung, Y.-B.; Cho, M.-S.; Tae, S.-H. Effect of supplementary cementitious materials on reduction of CO<sub>2</sub> emissions from concrete. *J. Clean. Prod.* **2015**, *103*, 774–783. [CrossRef]
21. Shen, W.; Liu, Y.; Yan, B.; Wang, J.; He, P.; Zhou, C.; Huo, X.; Zhang, W.; Xu, G.; Ding, Q. Cement industry of China: Driving force, environment impact and sustainable development. *Renew. Sustain. Energy Rev.* **2017**, *75*, 618–628. [CrossRef]
22. Zhao, X.; Liu, C.; Zuo, L.; Wang, L.; Zhu, Q.; Liu, Y.; Zhou, B. Synthesis and characterization of fly ash geopolymers for goaf backfill: Reuse of soda residue. *J. Clean. Prod.* **2020**, *260*, 121045. [CrossRef]
23. Song, W.; Zhu, Z.; Pu, S.; Wan, Y.; Huo, W.; Song, S.; Zhang, J.; Yao, K.; Hu, L. Synthesis and characterization of eco-friendly alkali-activated industrial solid waste-based two-component backfilling grouts for shield tunnelling. *J. Clean. Prod.* **2020**, *266*, 121974. [CrossRef]
24. Sahile, K. Utilization of Red Mud-Fly Ash Reinforced with Cement in Road Construction Applications. *Adv. Mater. Sci. Eng.* **2021**, *2021*, 3728652. [CrossRef]
25. Chen, M.; Wen, P.; Wang, C.; Chai, Z.; Gao, Z. Evaluation of particle size distribution and mechanical properties of mineral waste slag as filling material. *Constr. Build. Mater.* **2020**, *253*, 119183. [CrossRef]
26. Nguyen, T.K.V.; Doan, T.T.H.; Cao, T.H.; Pham, H.S. A Study of State Parameters for Road Construction of MSWI Bottom Ash. *Eng. Technol. Appl. Sci. Res.* **2021**, *11*, 7624–7627. [CrossRef]
27. Sukprasert, S.; Hoy, M.; Horpibulsuk, S.; Arulrajah, A.; Rashid, A.S.A.; Nazir, R. Fly ash based geopolymer stabilisation of silty clay/blasted furnace slag for subgrade applications. *Road Mater. Pavement Des.* **2019**, *22*, 357–371. [CrossRef]
28. Dong, F.; Xu, L.; Peng, T.; Dai, Q.; Chen, S. The mineralogy in the process of industrial solid wastes treatment and resource recycle. *Earth Sci. Front.* **2014**, *21*, 302–312. [CrossRef]
29. Lang, L.; Chen, B.; Chen, B. Strength evolutions of varying water content-dredged sludge stabilized with alkali-activated ground granulated blast-furnace slag. *Constr. Build. Mater.* **2021**, *275*, 122111. [CrossRef]
30. Mozejko, C.A.; Francisca, F.M. Enhanced mechanical behavior of compacted clayey silts stabilized by reusing steel slag. *Constr. Build. Mater.* **2020**, *239*, 117901. [CrossRef]
31. Lang, L.; Song, C.; Xue, L.; Chen, B. Effectiveness of waste steel slag powder on the strength development and associated micro-mechanisms of cement-stabilized dredged sludge. *Constr. Build. Mater.* **2020**, *240*, 117975. [CrossRef]
32. Huang, X.; Zhou, G. Utilization of industrial waste gypsum in soil stabilization. *Ind. Constr.* **1994**, *9*, 24–28. [CrossRef]
33. Ye, G.; Shu, H.; Zhang, Z.; Kang, S.; Zhang, S.; Wang, Q. Solidification and field assessment of soft soil stabilized by a waste-based binder using deep mixing method. *Bull. Eng. Geol. Environ.* **2021**, *80*, 5061–5074. [CrossRef]
34. Sun, R.; Fang, C.; Gao, F.; Ge, Z.; Zhang, H.; Lu, Q. Study on Pavement Performance and Solidified Mechanism of Solidified Soil Based on Solid Waste. *China J. Highw. Transp.* **2021**, *34*, 216–224. [CrossRef]
35. Mujtaba, H.; Aziz, T.; Farooq, K.; Sivakugan, N.; Das, B.M. Improvement in Engineering Properties of Expansive Soils using Ground Granulated Blast Furnace Slag. *J. Geol. Soc. India* **2018**, *92*, 357–362. [CrossRef]
36. Ji, X.; Hou, J.; Liu, Y.; Liu, J. Effect of CaO-FeO-MnO system solid solution on the hydration activity of tri-component f-CaO in steel slag. *Constr. Build. Mater.* **2019**, *225*, 476–484. [CrossRef]
37. Pu, S.; Zhu, Z.; Huo, W. Evaluation of engineering properties and environmental effect of recycled gypsum stabilized soil in geotechnical engineering: A comprehensive review. *Resour. Conserv. Recycl.* **2021**, *174*, 105780. [CrossRef]
38. Huang, Z.; Zhang, H. Spatial pattern analysis and influencing factors detection of general industrial solid waste in China. *J. Saf. Environ.* **2022**, *22*, 980–987.
39. Wang, Q.; Wang, D.; Zhuang, S. The soundness of steel slag with different free CaO and MgO contents. *Constr. Build. Mater.* **2017**, *151*, 138–146. [CrossRef]
40. Morel, J.-C.; Pkla, A.; Walker, P. Compressive strength testing of compressed earth blocks. *Constr. Build. Mater.* **2007**, *21*, 303–309. [CrossRef]
41. Jiang, B.; Xia, W.; Wu, T.; Liang, J. The optimum proportion of hygroscopic properties of modified soil composites based on orthogonal test method. *J. Clean. Prod.* **2020**, *278*, 123828. [CrossRef]
42. *JTG E51-2009*; Test Methods of Materials Stabilized with Inorganic Binders for Highway Engineering. China Communications Press: Beijing, China, 2009.
43. *AASHTO T 193-2013*; Standard Method of Test for The California Bearing Ratio. American Association of State Highway and Transportation Officials (AASHTO): Washington, DC, USA, 2013.
44. *ASTM D4843-88*; Standard Test Methods for Wetting and Drying Test of Solid Wastes. American Society for Testing Materials: Washington, DC, USA, 2009.
45. Wu, H.; Li, Z.; Song, W.; Zou, J.; Liu, W.; Yu, J. Experimental Study on Moisture Susceptibility of Subgrade Soil with Superabsorbent Polymers. *J. Mater. Civ. Eng.* **2019**, *31*, 04019120. [CrossRef]
46. *AASHTO T 307-99*; Standard Method of Test for Determining the Resilient Modulus of Soil and Aggregate Materials. American Association of State Highway Transportation Officials (AASHTO): Washington, DC, USA, 1999.
47. *ASTM D. 4695-03*; Standard Guide for General Pavement Deflection Measurements. American Society for Testing and Materials: Washington, DC, USA, 2003. Available online: [https://scholar.google.com/scholar\\_lookup?title=StandardGuideforGeneralPavementDeflectionMeasurements&author=ASTM&publication\\_year=2015](https://scholar.google.com/scholar_lookup?title=StandardGuideforGeneralPavementDeflectionMeasurements&author=ASTM&publication_year=2015) (accessed on 21 May 2022).
48. Mohammed, B.S.; Achara, B.E.; Nuruddin, M.F.; Yaw, M.; Zulkefli, M.Z. Properties of nano-silica-modified self-compacting engineered cementitious composites. *J. Clean. Prod.* **2017**, *162*, 1225–1238. [CrossRef]

49. Khan, M.I.; Sutanto, M.H.; Bin Napiah, M.; Khan, K.; Rafiq, W. Design optimization and statistical modeling of cementitious grout containing irradiated plastic waste and silica fume using response surface methodology. *Constr. Build. Mater.* **2020**, *271*, 121504. [[CrossRef](#)]
50. Zahid, M.; Shafiq, N.; Isa, M.H.; Gil, L. Statistical modeling and mix design optimization of fly ash based engineered geopolymer composite using response surface methodology. *J. Clean. Prod.* **2018**, *194*, 483–498. [[CrossRef](#)]
51. Achara, B.E.; Mohammed, B.S.; Liew, M. Bond behaviour of nano-silica-modified self-compacting engineered cementitious composite using response surface methodology. *Constr. Build. Mater.* **2019**, *224*, 796–814. [[CrossRef](#)]
52. Pooni, J.; Robert, D.; Giustozzi, F.; Setunge, S.; Xie, Y.; Xia, J. Performance evaluation of calcium sulfoaluminate as an alternative stabilizer for treatment of weaker subgrades. *Transp. Geotech.* **2021**, *27*, 100462. [[CrossRef](#)]
53. Hassan, N.; Hassan, W.H.W.; Rashid, A.S.A.; Latifi, N.; Yunus, N.Z.M.; Horpibulsuk, S.; Moayedi, H. Microstructural characteristics of organic soils treated with biomass silica stabilizer. *Environ. Earth Sci.* **2019**, *78*, 367. [[CrossRef](#)]
54. Pu, S.; Zhu, Z.; Wang, H.; Song, W.; Wei, R. Mechanical characteristics and water stability of silt solidified by incorporating lime, lime and cement mixture, and SEU-2 binder. *Constr. Build. Mater.* **2019**, *214*, 111–120. [[CrossRef](#)]
55. Pu, S.Y.; Zhu, Z.D.; Song, W.L.; Wan, Y.; Wang, H.R.; Song, S.G.; Zhang, J. Mechanical and Microscopic Properties of Cement Stabilized Silt. *KSCE J. Civ. Eng.* **2020**, *24*, 2333–2344. [[CrossRef](#)]
56. Ren, C.; Wang, W.; Li, G. Preparation of high-performance cementitious materials from industrial solid waste. *Constr. Build. Mater.* **2017**, *152*, 39–47. [[CrossRef](#)]
57. Wu, S.; Yao, Y.; Yao, X.; Ren, C.; Li, J.; Xu, D.; Wang, W. Co-preparation of calcium sulfoaluminate cement and sulfuric acid through mass utilization of industrial by-product gypsum. *J. Clean. Prod.* **2020**, *265*, 121801. [[CrossRef](#)]
58. Yao, Y.; Wang, W.; Ge, Z.; Ren, C.; Yao, X.; Wu, S. Hydration study and characteristic analysis of a sulfoaluminate high-performance cementitious material made with industrial solid wastes. *Cem. Concr. Compos.* **2020**, *112*, 103687. [[CrossRef](#)]